To be submitted to *Advanced Batteries and Supercapacitors* (The Electrochemical Society Proceedings Series, **PV 2001-21**), the 2001 Joint International Meeting: the 200th Meeting of The Electrochemical Society and the 52nd Meeting of the International Society of Electrochemistry, September 2-7,001, San Francisco, CA

Li Diffusion and High-Voltage Cycling Behavior of Thin-Film $LiCoO_2$ Cathodes

Young-Il Jang and Nancy J. Dudney

Solid State Division
Oak Ridge National Laboratory, P.O. Box 2008
Oak Ridge, Tennessee 37831-6030

Prepared by
SOLID STATE DIVISION
OAK RIDGE NATIONAL LABORATORY
Managed by
UT-BATTELLE, LLC.
under
Contract No. DE-AC-05-00OR22725
with the
U.S. DEPARTMENT OF ENERGY
Oak Ridge, Tennessee

September 2001

Li DIFFUSION AND HIGH-VOLTAGE CYCLING BEHAVIOR OF THIN-FILM $LiCoO_2$ CATHODES

Young-Il Jang and Nancy J. Dudney
Solid State Division, Oak Ridge National Laboratory
Oak Ridge, Tennessee 37831-6030, USA

Mass transport and thermodynamic properties of Li_xCoO_2 were studied by the potentiostatic intermittent titration technique (PITT) using solid-state thin-film batteries that provide a well-defined diffusion geometry. Both the chemical diffusion coefficient and the thermodynamic factor have minima at the phase boundaries of the Li/vacancy ordered phase "$Li_{0.5}CoO_2$". The self-diffusion coefficient of Li has a minimum at $x = 0.5$ associated with the Li/vacancy ordering. As the degree of ordering increases, the nonmonotonic variations become more pronounced when approaching $x = 0.5$ in Li_xCoO_2. We also show that thin-film $LiCoO_2$ cathodes having grains of sub-micrometer size combined with the Lipon electrolyte exhibit excellent capacity retention when charged up to 4.5 V.

INTRODUCTION

High-power applications of rechargeable Li batteries require fast Li ion mobility within intercalation compounds. The α-$NaFeO_2$ structure of $LiCoO_2$ ensures a high chemical diffusion coefficient of Li (D_C) and in turn, a high rate capability. The structure is based on a nearly cubic-close-packed arrangement of oxygen ions with Li ions and Co ions alternatively occupying the octahedral sites between adjacent oxygen ion layers (space group $R\bar{3}m$) (1). The values of D_C in the literature vary from 10^{-13} to 10^{-7} cm^2/sec (2-16). This large difference is attributed to different assumptions for the geometrical factors (diffusion length and cross-sectional surface area) used in the calculation of D_C (13,14). In terms of both geometry and feasibility, thin-film electrodes combined with solid electrolytes are ideal for diffusion studies (17).

Extraction of Li from $LiCoO_2$ occurs via several phase transitions. In Li_xCoO_2, two hexagonal phases coexist for $0.75 \leq x \leq 0.93$ (18), which has been attributed to the insulator-metal transition upon Li extraction (19,20). At compositions near $Li_{0.5}CoO_2$, Li ions are ordered in rows separated by rows of vacancies within the Li layers (18). This is accompanied by a lattice distortion to a monoclinic symmetry (space group $P2/m$) (18,21,22). A recent first-principles calculation has predicted that D_C and the self diffusion coefficient of Li (D_S) have a minimum at $x = 0.5$ due to Li ordering (23), however, no such minimum has been observed at $x = 0.5$ in previous studies (5,7,13,14,16).

Reversible delithiation in commercial Li_xCoO_2 batteries is typically limited to $x \sim 0.5$ (corresponding to ~4.2 V vs. Li), which has been attributed to mechanical failure associated with the large change in the c parameter for $x < 0.5$ (24). It has been suggested that electrochemical grinding above 4.2 V results in capacity loss as well as cobalt dissolution in non-aqueous liquid electrolyte (25). To increase the capacity and energy

density utilization, efforts have been made to enhance the cycling stability to voltages above 4.2 V by surface treatment or doping of $LiCoO_2$ powders (26-29). Even though such approaches can improve the capacity retention at high voltages, it generally incurs high synthesis costs or lower specific capacities.

In this study, we employed solid-state thin-film Li batteries with Li_xCoO_2 cathodes in order to measure D_C based on a better-defined geometry than conventional powder cathodes. We prepared Li_xCoO_2 cathodes showing different degrees of ordering in order to elucidate the effect of Li ordering on D_C and D_S. The diffusion coefficients were determined by the potentiostatic intermittent titration technique (PITT) (30,31). Here we report that D_S does show a minimum at $x = 0.5$ with the minimum becoming clearer as the degree of ordering increases. We discuss the effect of Li ordering on D_C and the thermodynamic factor of Li (Θ). We also show that thin-film $LiCoO_2$ batteries exhibit excellent capacity retention when charged up to 4.5 V. We discuss the cycling stability of thin-film $LiCoO_2$ cathodes in high voltage ranges based on the strain and grain size effects.

EXPERIMENTAL

Thin-film batteries with $LiCoO_2$ cathodes were fabricated as detailed elsewhere (17,32). Pt and Ni films deposited on polycrystalline Al_2O_3 plates were used as the cathode and anode current collectors, respectively. Cathode films were deposited by radio frequency (rf) magnetron sputtering of $LiCoO_2$ targets in an Ar-O_2 atmosphere and annealed at 700-800°C for 2 h in O_2. The electrolyte was amorphous lithium phosphorus oxynitride (Lipon) of 1.5 μm thickness. Thermally vapor-deposited Li metal was used as the anode. For the study of Li diffusion, we fabricated two batteries (*A* and *B*) with $LiCoO_2$ cathodes showing different degrees of Li-vacancy ordering in the voltage range between 4.05 and 4.2 V. The cathode thickness determined by profilometry and direct observation of the fractured cell in a scanning electron microscope was 2.6±0.2 μm. This value was used for the diffusion length. The thickness of cathodes used for the study of high-voltage cycling behavior was 1.0±0.1 μm.

Electrochemical characterization of the batteries was performed at 25°C using Maccor battery test systems. For the study of Li diffusion, PITT measurements were performed after the initial 20 cycles between 3.0 and 4.2 V. We applied a potential step of 10 mV and measured the current as a function of time. The current decayed as the Li ions diffused through the cathode film. When the current reached 0.5 $\mu A/cm^2$, the potential was stepped to the next level. This procedure was repeated between 3.86 and 4.2 V at both increasing and decreasing potentials, corresponding to Li deintercalation and intercalation, respectively. For the study of high-voltage cycling behavior, the batteries were first cycled 3 times between 3.0 and 4.2 V at 5 $\mu A/cm^2$, followed by cycling at 0.1 mA/cm^2 with various charge cutoff voltages of 4.2-4.5 V. Discharge cutoff voltage was fixed at 3.0 V. To monitor change in cell resistance during cycling, discharge was also performed between 3.0 and 4.2 V at various current densities of 0.1, 0.3, 0.5, 0.7, and 1 mA/cm^2. For each cycle, the batteries were charged at 0.1 mA/cm^2 to a cutoff voltage and then held at the voltage until the current decreased to $<1\ \mu A/cm^2$.

RESULTS AND DISCUSSION

Li Diffusion

Figures 1(a) and (b) show the incremental capacity ($\Delta Q/\Delta V$) obtained by PITT at 25°C using the cells *A* and *B*, respectively. The incremental capacity is the capacity accumulated on each potential step divided by the size of the potential step. The major peak denoted "*a*" at ~3.9 V corresponds to a first-order transition between two hexagonal phases (18,21). Two minor peaks ("*b*" and "*c*") are also seen above 4 V (see upper insets), which are associated with order-disorder transitions at compositions near $Li_{0.5}CoO_2$ (18). A deep minimum between the two peaks is a qualitative indicator of the degree of Li ordering around $Li_{0.5}CoO_2$ (33). Figure 1 shows that cell *A* has higher peaks and a deeper minimum than cell *B*. This suggests that the degree of Li ordering in the cathode of cell *A* is higher than that of *B*.

The lower insets of Fig. 1 show the titration curves obtained by integrating the incremental capacities. Here we normalized our data so that the minimum in $\Delta Q/\Delta V$ falls at $x = 0.5$ and so that $x = 1.0$ corresponds to $V = 3.84$ V, based on the phase diagram of Li_xCoO_2 in Ref. 18. Peaks in the plot of $\Delta Q/\Delta V$ vs. voltage appear as plateaus in the plot of voltage vs. x in Li_xCoO_2.

In the composition range of $0.45 < x < 0.7$ where Li_xCoO_2 exists as a single phase having either a hexagonal or a monoclinic structure, the current during each potential step decayed exponentially with time following an initial rapid increase. For example, Fig. 2(a) shows the time dependence of the current in the cell *A* when the voltage was increased from 3.985 to 3.995 V. At long time, the expression for the current (I) as a function of time (t) is known to be (14,31):

$$I(t) = \frac{2FS(C_S - C_O)D_C}{L} \exp(-\frac{\pi^2 D_C t}{4L^2}) \qquad [1]$$

Here F is the Faraday constant, S the cross-sectional area common to both the electrolyte and the cathode, L the thickness of the cathode film, and (C_S-C_O) the change in Li concentration at the cathode-electrolyte interface during each potential step. We calculated D_C from the slope of the linear region in the plot of $\ln I(t)$ vs. t (see inset of Fig. 2(a)).

In the two-phase region ($0.93 > x > 0.75$), the current decay showed multiple-staged transient behavior. This is demonstrated in Fig. 2(b) where the voltage of the cell *A* was increased from 3.915 to 3.925 V. Such a transient behavior is attributed to a phase boundary movement in the two-phase region (34). As the phase boundary movement involves two diffusion terms associated with each phase (35), D_C cannot be determined as a single value in the two-phase region.

Figures 3(a) and (d) show the plots of D_C vs. x of Li_xCoO_2 for the cells *A* and *B*, respectively. Uncertainty in thickness of the cathode films largely determined the uncertainty of D_C, denoted by error bars in Figs. 3(a) and (d). The value of D_C ranges from 4×10^{-11} from 3×10^{-10} cm^2/s in the composition range of $0.45 < x < 0.7$, in agreement with previous results obtained using thin-film cathodes or powder electrodes

with the diffusion length determined by the particle size (9,12-14). These results suggest that the early data of D_C on the order of 10^{-9}-10^{-6} cm^2/s were overestimated by neglecting the permeation of liquid electrolyte into powder electrodes and carbon additives that shorten the actual diffusion lengths.

D_C monotonically increases as x decreases from 0.7 to 0.55, consistent with the previous reports (3,5,13,14). However, in the composition range near $Li_{0.5}CoO_2$ ($0.45 < x < 0.55$), variation of D_C with x is more complex. Note that the plot of D_C vs. x shows two minima at x = 0.53 and 0.48 (Fig. 3(a)). These compositions correspond to peaks "*b*" and "*c*" in the incremental capacity plot (Fig. 1(a)), which are associated with the order-disorder transitions at compositions near $Li_{0.5}CoO_2$ as mentioned above.

Assuming that the transport phenomena in Li_xCoO_2 is dominated by Li ions and electrons, D_C can be expressed as a product of D_S, Θ, and the electronic transference number (t_e) (36). As Li_xCoO_2 ($0.45 < x < 0.7$) is predominantly an electronic conductor (19,20), so that $t_e \approx 1$, we have simply:

$$D_C = D_S\Theta = D_S \frac{\partial \ln a_{Li}}{\partial \ln c_{Li}} \qquad [2]$$

Θ can be determined independently from the titration curves according to the following expression (31):

$$\Theta = \frac{\P \ln a_{Li}}{\P \ln c_{Li}} = -\frac{Fx}{RT}\frac{dV}{dx} \qquad [3]$$

Here V is the voltage, R the gas constant, and T the absolute temperature. We calculated $-dV/dx$ from the lower insets of Fig. 1 and plotted Θ vs. x of Li_xCoO_2 for the cells *A* and *B* in Figs. 3(b) and (e), respectively. Interestingly, the x dependence of Θ is similar to that of D_C, suggesting that the latter is mainly determined by the former. Like $\Delta Q/\Delta V$ in Fig. 1, $-dx/dV$ has local maxima at the phase boundaries (not shown here), therefore, Θ and, in turn, D_C have minima at the phase boundaries represented by the dashed lines in Fig. 3. As evident from Fig. 3, the cell *A* exhibits more pronounced minima in both D_C and Θ than the cell *B*. Because the cell *A* has a higher degree of ordering than the cell *B*, it is clear that the existence of minima in D_C and Θ is associated with the order-disorder transitions.

We calculated D_S using Eq. 3; the results are shown in Figs. 3(c) and (f) as a function of x in Li_xCoO_2 for the cells *A* and *B*, respectively. The uncertainties in D_S are large, but nearly a constant over the entire composition range. Note in Fig. 3(c) that D_S has a minimum at x = 0.5, consistent with the prediction of Ref. 5. As discussed in Ref. 23, the occurrence of this minimum is attributed to a higher activation energy associated with Li jumps in ordered $Li_{0.5}CoO_2$. Comparing Fig. 3(c) with (f), the well-ordered $Li_{0.5}CoO_2$ cathode of *A* exhibits a more pronounced minimum in D_S than the less-ordered cathode of *B*. The minimum in D_S is barely seen in Fig. 3(f), suggesting that the activation energy barrier confining the Li ions to ordered sites is lower in the disordered

$Li_{0.5}CoO_2$. Note that the minimum in D_S at $x = 0.5$ in Fig. 3(c) is less pronounced than the predicted minimum in Ref. 23 by two orders of magnitude. This can be explained by less-than-perfect Li-vacancy ordering. As D_S is a product of D_S and Θ, a reduced minimum in D_S can result in a reduced minimum in D_C. As Θ has a maximum at $x = 0.5$, a reduced minimum in D_S can even result in a maximum as shown in Fig. 3.

From the values of D_S in our result, the partial ionic conductivity of Li (σ_{Li}) can be calculated using the Nernst-Einstein equation (37). σ_{Li} is determined to be $\approx 10^{-6}$ S/cm in the composition range of this study. As the total electrical conductivity is ≈10 S/cm in this composition range (20), the ionic transference number of Li (t_{Li}) is determined to be $\approx 10^{-7}$.

High-Voltage Cycling Behavior

Figure 4 shows the charge-discharge curves of a cell cycled at 0.1 mA/cm^2 in various voltage ranges. The charge cutoff voltage was varied between 4.2 and 4.5 V, while the discharge cutoff voltage was fixed at 3.0 V. Inset of Fig. 4 shows the corresponding differential capacity plots during charge and discharge. Peaks "*a*" and "*b*" are associated with the order-disorder phase transitions at compositions around $Li_{0.5}CoO_2$ (18). The heights of peaks "*a*" and "*b*" and the depth of minimum between the peaks do not change significantly with cycling. This indicates that the degree of Li/vacancy ordering in the monoclinic phase remains almost constant even after cycling between 3.0 and 4.5 V. Inset of Fig. 4 shows that an additional peak starts to develop at >4.4 V, marked "*c*". The peak "*c*" is attributed to formation of a second phase. Ohzuku and Ueda (21) and Amatucci *et al*. (38) reported that the two-phase region at ~4.5 V ($0.15 < x < 0.25$ in Li_xCoO_2) consists of a hexagonal phase and a monoclinic phase due to the Jahn-Teller distortion associated with low-spin Co^{4+} ions, while Yang *et al*. (39) reported that the two-phase region consists of two hexagonal phases.

Figure 5 shows the discharge capacity of the cell in the various voltage ranges. Table I shows the capacity fade per cycle in percentage of the initial discharge capacity in each voltage range. We determined the capacity fade rate by linear regression for each voltage range. The cell exhibits excellent cyclability with a capacity fade rate of ≤0.04% per cycle when charged up to 4.5 V. By extending the charge cutoff voltage from 4.2 to 4.5 V, the discharge capacity and energy density utilization increased by 35% and 38%, respectively, at 0.1 mA/cm^2. Considering previous results in the literature, such a degree of capacity retention is remarkably high for $LiCoO_2$ cathodes in the high voltage range. For example, uncoated $LiCoO_2$ powders in Refs. 27 ad 28 retained only 47% of the initial capacity after 50 cycles between 2.75 and 4.4 V at 0.5*C* rate (1*C* = 140 mA/g). In the present work, a thin-film $LiCoO_2$ cathode retained 98% of the initial capacity after 100 cycles between 3.0 and 4.4 V at 0.1 mA/cm^2, corresponding to 0.7*C* rate (see Fig. 6). In general, capacity fade appears to be more rapid when measured at higher current densities. We can therefore conclude that our thin-film $LiCoO_2$ cathodes clearly show excellent capacity retention compared to conventional powder samples.

Generally, fracture of electrochemically active materials occurs during cycling unless the strain is zero such that the lattice dimensions do not change during the Li insertion and extraction (40). However, electrochemical cycling behavior is significantly improved when the initial particle size is very small (41). Huggins and Nix reported that

there is a critical particle size (d_C) below which fracture does not occur (42). It was previously reported that when $LiCoO_2$ particles of 0.5 μm size were cycled between 2.5 and 4.35 V, approximately 20% of examined particles were fractured (43). Approximately 80% of the initial capacity was retained after 50 cycles in Ref. 43. The grain size of the present thin-film $LiCoO_2$ cathodes was determined to be 0.2-0.3 μm by scanning electron microscopy (see Fig. 7). Therefore, it can be suggested that 0.3 μm < d_C < 0.5 μm for $LiCoO_2$ with 1.8% change in the *c* parameter when charged up to 4.4 V. For direct observation of cycled cathode films, TEM study is in progress.

CONCLUSIONS

The chemical diffusion coefficient (D_C) and the thermodynamic factor (Θ) of Li were determined by the potentiostatic intermittent titration technique (PITT) in the single-phase regions of Li_xCoO_2 ($0.45 < x < 0.7$). In order to provide a well-defined diffusion geometry, we used solid-state thin-film batteries in this study. Both D_C and Θ monotonically increase with decreasing x for $0.7 > x > 0.55$, but then vary with x in a more complex pattern in the composition range near $Li_{0.5}CoO_2$. Minima in D_C and Θ were observed at the phase boundaries of the Li-vacancy ordered phase $Li_{0.5}CoO_2$. From D_C and Θ, we calculated the self-diffusion coefficient of Li (D_S) as a function of x. D_S has a minimum at $x = 0.5$. The variations of D_C, Θ, and D_S near the composition of $Li_{0.5}CoO_2$ become more pronounced as the degree of Li-vacancy ordering increases in $Li_{0.5}CoO_2$.

We show that thin-film $LiCoO_2$ batteries exhibit excellent capacity retention when charged up to 4.5 V. The cycling stability of thin-film cathodes in the high voltage ranges can be explained based on the strain and grain size effects. It is suggested that the critical particle size (d_C) for $LiCoO_2$ below which fracture does not occur is that 0.3 μm < d_C < 0.5 μm. Significant increase in discharge capacity and energy density utilization has been achieved by extending the charge cutoff voltage from 4.2 to 4.5 V (35% and 38%, respectively, at 0.7*C* rate). The present study exemplifies the usefulness of a thin-film approach in developing $LiCoO_2$ batteries with higher capacity and energy density by enhancing the high-voltage cycling stability.

ACKNOWLEDGMENTS

Y.I.J. acknowledges a Eugene P. Wigner fellowship from the Oak Ridge National Laboratory. This research was sponsored by the U.S. Department of Energy's Division of Materials Sciences and Division of Chemical Sciences under contract DE-AC05-00OR22725 with the Oak Ridge National Laboratory, managed by UT-Battelle, LLC.

REFERECES

1. W. D. Johnston, R. R. Heikes, and D. Sestrich, *J. Phys. Chem. Solids*, 7, 1 (1958).
2. K. Mizushima, P. C. Jones, P. J. Wiseman, and J. B. Goodenough, *Mater. Res. Bull.*,

15, 783 (1980).
3. A. Honders, J. M. der Kinderen, A. H. van Heeren, J. H. W. de Wit, and G. H. J. Broers, *Solid State Ionics*, **15**, 265 (1985).
4. M. G. S. R. Thomas, P. G. Bruce, and J. B. Goodenough, *Solid State Ionics*, **17**, 13 (1985).
5. Y.-M. Choi, S.-I. Pyun, J.-S. Bae, and S.-I. Moon, *J. Power Sources*, **56**, 25 (1995).
6. C. H. Chen, A. A. J. Buysman, E. M. Kelder, and J. Schoonman, *Solid State Ionics*, **80**, 1 (1995).
7. J. Barker, R. Pynenburg, R. Koksbang, and M. Y. Saidi, *Electrochim. Acta*, **41**, 2481 (1996).
8. B. Garcia, J. Farcy, J. P. Pereira-Ramos, and N. Baffier, *J. Electrochem. Soc.*, **144**, 1179 (1997).
9. P. Birke, W. F. Chu, and W. Weppner, *Solid State Ionics*, **93**, 1 (1997).
10. H. Sato, D. Takahashi, T. Nishina, and I. Uchida, *J. Power Sources*, **68**, 540 (1997).
11. R. Alcántara, P. Lavela, J. L. Tirado, E. Zhecheva, and R. Stoyanova, *J. Electroanal. Chem.*, **454**, 173 (1998).
12. D. Aurbach, M. D. Levi, E. Levi, H. Teller, B. Markovsky, G. Salitra, U. Heider, and L. Heider, *J. Electrochem. Soc.*, **145**, 3024 (1998).
13. M. D. Levi, G. Salitra, B. Markovsky, H. Teller, D. Aurbach, U. Heider, and L. Heider, *J. Electrochem. Soc.*, **146**, 1279 (1999).
14. J. M. McGraw, C. S. Bahn, P. A. Parilla, J. D. Perkins, D. W. Readey, and D. S. Ginley, *Electrochim. Acta*, **45**, 187 (1999).
15. K. Dokko, S. Horikoshi, M. Nishizawa, T. Itoh, T. Abe, and I. Uchida, in *Lithium Batteries*, S. Surampudi, R. A. Marsh, Z. Ogumi, and J. Prakash, Editors, PV 99-25, p. 290, The Electrochemical Society Proceedings Series, Pennington, NJ (2000).
16. J.-S. Hong and J. R. Selman, *J. Electrochem. Soc.*, **147**, 3190 (2000).
17. Y.-I. Jang, B. J. Neudecker, and N. J. Dudney, *Electrochem. Solid-State Lett.*, **4**, A74 (2001).
18. J. N. Reimers and J. R. Dahn, *J. Electrochem. Soc.*, **139**, 2091 (1992).
19. A. Van der Ven, M. K. Aydinol, G. Ceder, G. Kresse, and J. Hafner, *Phys. Rev.*, B **58**, 2975 (1998)
20. M. Ménétrier, I. Saadoune, S. Levasseur, and C. Delmas, *J. Mater. Chem.*, **9**, 1135 (1999).
21. T. Ohzuku and A. Ueda, *J. Electrochem. Soc.*, **141**, 2972 (1994).
22. M. Catti, *Phys. Rev.*, B **61**, 1795 (2000).
23. A. Van der Ven and G. Ceder, *Electrochem. Solid-State Lett.*, **3**, 301 (2000).
24. T. Ohzuku, A Ueda, M. Nagayama, Y. Iwakoshi, and H. Komori, *Electrochim. Acta*, **38**, 1159 (1993).
25. G. G. Amatucci, J. M. Tarascon, and L. C. Klein, *Solid State Ionics*, **83**, 167 (1996).
26. E. Endo, T. Yasuda, A. Kita, K. Yamaura, and K. Sekai, *J. Electrochem. Soc.*, **147**, 1291 (2000).
27. J. Cho, C.-S. Kim, and S.-I. Yoo, *Electrochem. Solid-State Lett.*, **3**, 362 (2000).
28. J. Cho, Y. J. Kim, and B. Park, *Chem. Mater.*, **12**, 3788 (2000).
29. S.-T. Myung, N. Kumagai, S. Komaba, and H.-T. Chung, *Solid State Ionics*, **139**, 47 (2001).
30. A. H. Thompson, *J. Electrochem. Soc.*, **126**, 608 (1979).
31. C. J. Wen, B. A. Boukamp, R. A. Huggins, and W. Weppner, *J. Electrochem. Soc.*, **126**, 2258 (1979).
32. B. Wang, J. B. Bates, F. X. Hart, B. C. Sales, R. A. Zuhr, and J. D. Robertson, *J.*

Electrochem. Soc., **143**, 3203 (1996).
33. J. N. Reimers, J. R. Dahn, and U. von Sacken, *J. Electrochem. Soc.*, **140**, 2752 (1993).
34. Y.-M. Choi, S.-I. Pyun, and J. M. Paulsen, *Electrochim. Acta*, **44**, 623 (1998).
35. P. Shewmon, *Diffusion in Solids*, 2nd Ed., The Minerals, Metals & Materials Society, Pennsylvania (1989).
36. W. Weppner and R. A. Huggins, *J. Electrochem. Soc.*, **124**, 1569 (1977).
37. H. Rickert, *Electrochemistry of Solids*, Springer-Verlag, New York (1982).
38. G. G. Amatucci, J. M. Tarascon, and L. C. Klein, *J. Electrochem. Soc.*, **143**, 1114 (1996).
39. X. Q. Yang, X. Sun, and J. McBreen, *Electrochem. Comm.*, **2**, 100 (2000).
40. T. Ohzuku and A. Ueda, *Solid State Ionics*, **69**, 201 (1994).
41. J. Yang, M. Winter, and J. O. Besenhard, *Solid State Ionics*, **90**, 281 (1996).
42. R. A. Huggins and W. D. Nix, *Ionics*, **6**, 57 (2000).
43. H. Wang, Y.-I. Jang, B. Huang, D. R. Sadoway, and Y.-M. Chiang, *J. Electrochem. Soc.*, **146**, 473 (1999).

Table I. Capacity fade per cycle determined by linear regression for each voltage range. The capacity fade is given in percentage of the initial discharge capacity in each voltage range. The charge cutoff voltage was varied from 4.2 to 4.5 V, while the discharge cutoff voltage was fixed at 3.0 V. All the cycles were performed at 0.1 mA/cm^2 at 25°C.

charge cutoff voltage (V)	4.2	4.25	4.3	4.35	4.4	4.45	4.5	4.2
capacity fade per cycle (%)	0.0051 ±0.0004	0.005 ±0.001	0.0085 ±0.0005	0.0075 ±0.0007	0.0120 ±0.0008	0.0246 ±0.0009	0.0447 ±0.0007	0.0097 ±0.0007

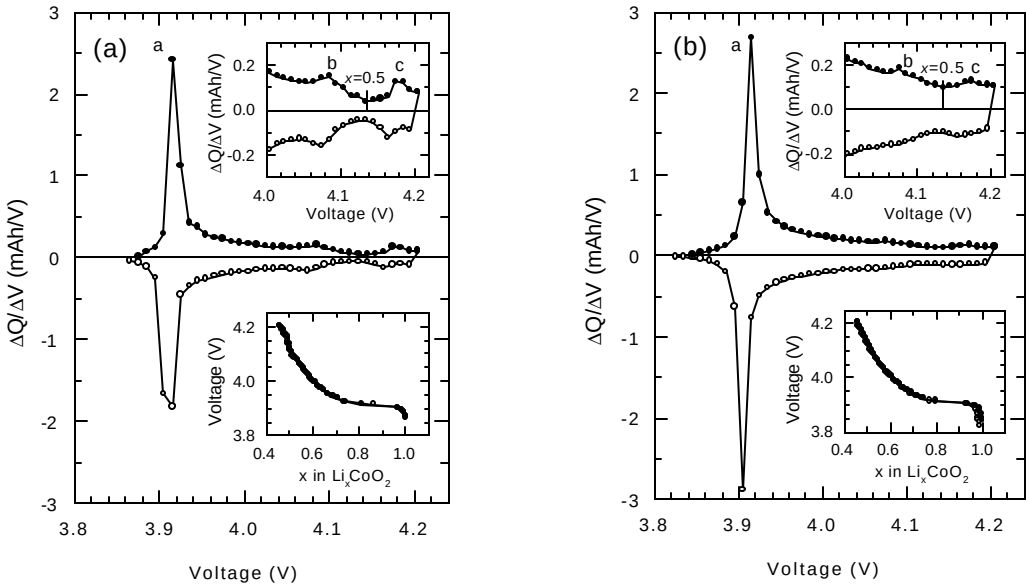

Figure 1. Incremental capacities ($\Delta Q/\Delta V$) obtained by the potentiostatic intermittent titration technique (PITT) at 25°C using the cells (a) *A* and (b) *B*. Refer to the text regarding the peak denotations. Lower insets show the titration curves obtained by integrating the incremental capacities.

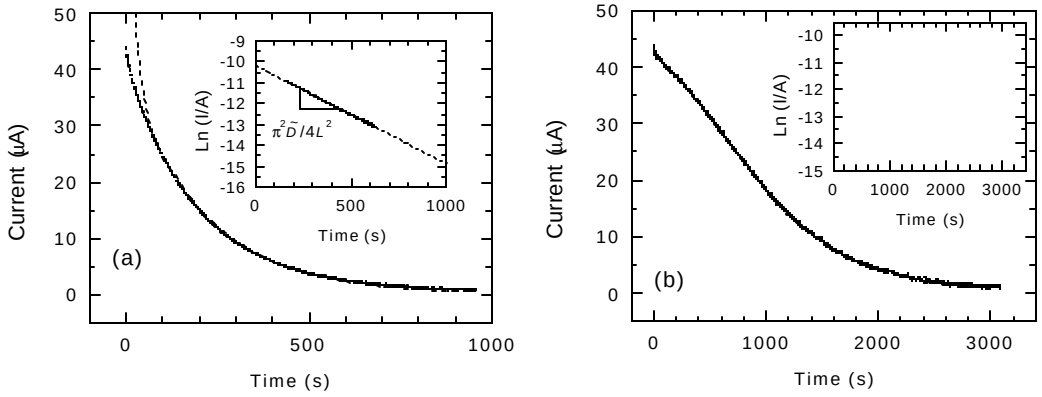

Figure 2. Time dependence of the current in the cell *A* (a) when the voltage was increased from 3.985 to 3.995 V and (b) when the voltage was increased from 3.915 to 3.925 V.

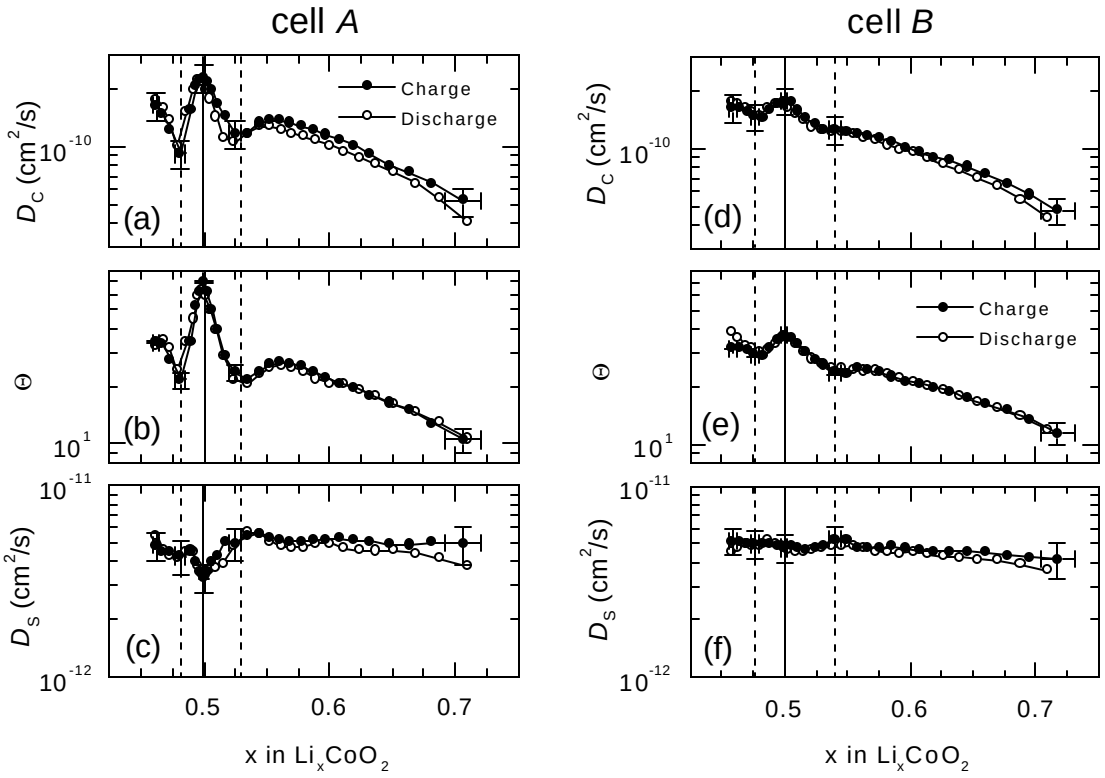

Figure 3. Compositional variation of (a)(d) chemical diffusion coefficient of Li (D_C); (b)(e) thermodynamic factor of Li (Θ); and (c)(f) self diffusion coefficient of Li (D_S) obtained by the potentiostatic intermittent titration technique (PITT) at 25°C. The ordinates are on a logarithmic scale. The dashed lines indicate the phase boundaries of the Li-vacancy ordered phase. (a), (b), and (c) correspond to cell *A*, while (d), (e), and (f) cell *B*.

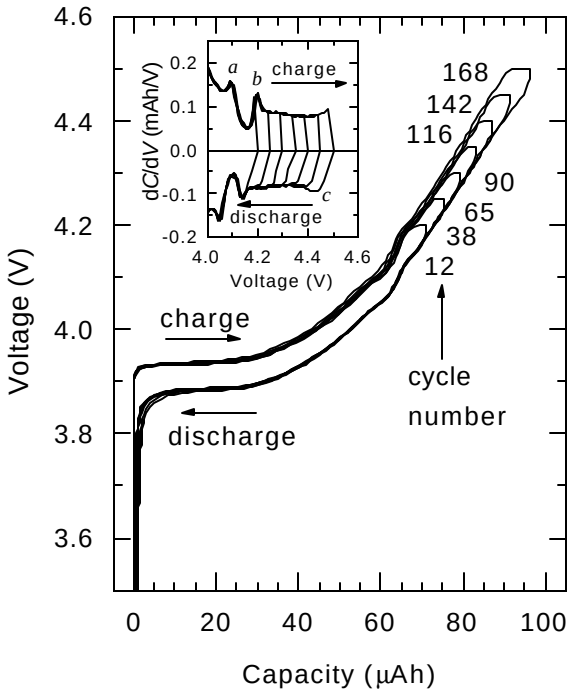

Figure 4. Charge-discharge curves with the various charge cutoff voltages of 4.2, 4.25, 4.3, 4.35, 4.4, 4.45, and 4.5 V. The discharge cutoff voltage was fixed at 3.0 V. All the cycles were performed at 0.1 mA/cm^2 at 25°C. Inset shows the corresponding differential capacity plots during charge and discharge.

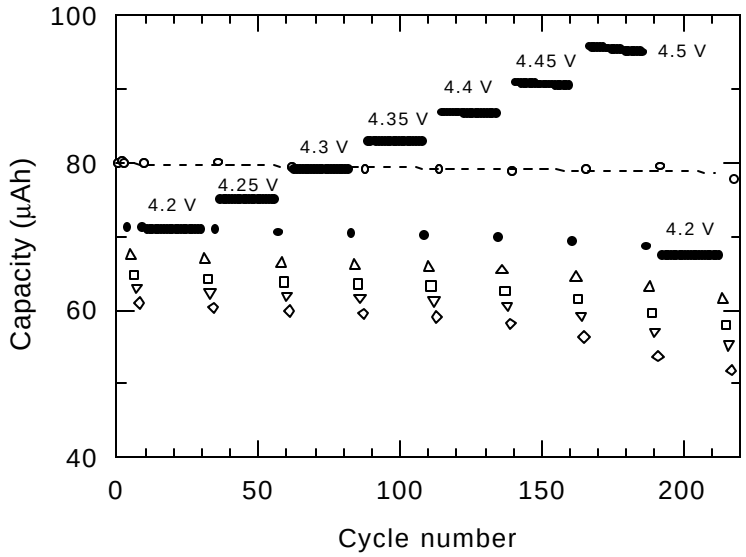

Figure 5. Discharge capacities with the various charge cutoff voltages of 4.2, 4.25, 4.3, 4.35, 4.4, 4.45, and 4.5 V. The discharge cutoff voltage was fixed at 3.0 V. All the cycles were performed at 25°C. (●: 0.1 mA/cm^2 in various voltage ranges; ○, Δ, □, ∇, and ◇ correspond to 0.005, 0.3, 0.5, 0.7, and 1.0 mA/cm^2 between 3.0 and 4.2 V, respectively.)

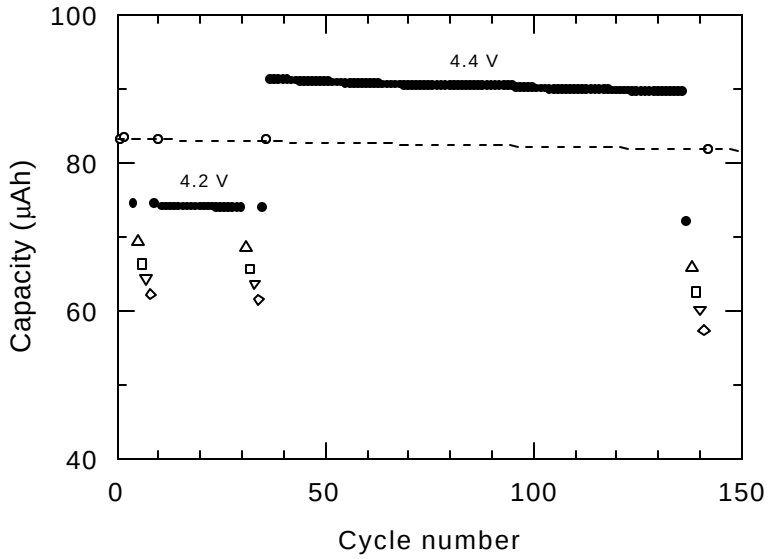

Figure 6. Discharge capacities with charge cutoff voltages of 4.2 and 4.4 V. The discharge cutoff voltage was fixed at 3.0 V. All the cycles were performed at 25°C. Capacity fade rate per cycle in each voltage range is noted percentage. (●: 0.1 mA/cm^2 in various voltage ranges; ○, Δ, □, ∇, and ◇ correspond to 0.005, 0.3, 0.5, 0.7, and 1.0 mA/cm^2 between 3.0 and 4.2 V, respectively.)

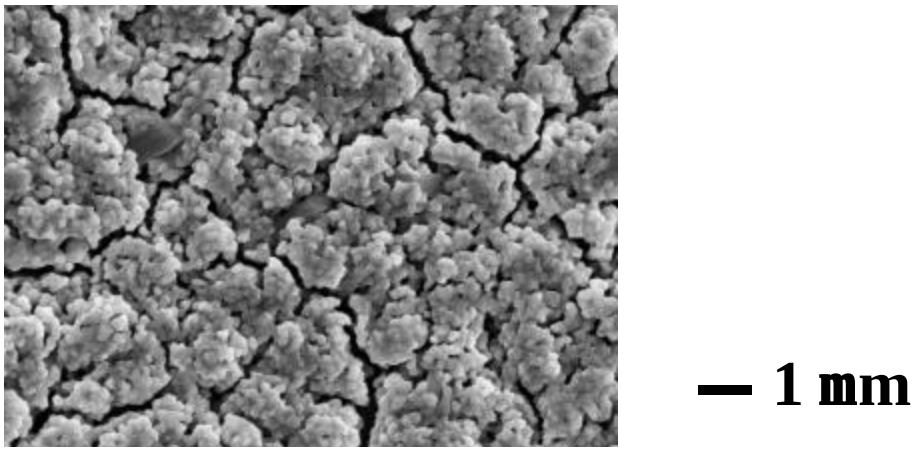

Figure 7. Plan-view SEM micrograph of $LiCoO_2$ cathode film.

KEY WORDS

$LiCoO_2$

Lipon

Thin-film batteries

Diffusion

Potentiostatic intermittent titration technique (PITT)